Clathrin Heavy Chain Subunits Coordinate Endo- and Exocytic Traffic and Affect Stomatal Movement[1][CC-BY]

Emily R. Larson,[a,2] Eva Van Zelm,[a,b] Camille Roux,[c] Annie Marion-Poll,[c] and Michael R. Blatt[a]

[a]Laboratory of Plant Physiology and Biophysics, University of Glasgow, Glasgow G12 8QQ, United Kingdom
[b]University of Amsterdam, Faculty of Science, Graduate School of Life and Earth Sciences, 1090 GE Amsterdam, The Netherlands
[c]Institut Jean-Pierre Bourgin, Institut National de la Recherche Agronomique, AgroParisTech, Centre National de la Recherche Scientifique, Université Paris-Saclay, 78000 Versailles, France

ORCID IDs: 0000-0002-5498-8152 (E.R.L.); 0000-0003-1217-0739 (E.V.Z.); 0000-0003-1733-1984 (A.M.-P.); 0000-0003-1361-4645 (M.R.B.).

The current model for vesicular traffic to and from the plasma membrane is accepted, but the molecular requirements for this coordination are not well defined. We have identified the *hot ABA-deficiency suppressor1* mutant, which has a stomatal function defect, as a *clathrin heavy chain1* (*CHC1*) mutant allele and show that it has a decreased rate of endocytosis and growth defects that are shared with other *chc1* mutant alleles. We used *chc1* alleles and the related *chc2* mutant as tools to investigate the effects that clathrin defects have on secretion pathways and plant growth. We show that secretion and endocytosis at the plasma membrane are sensitive to CHC1 and CHC2 function in seedling roots and that *chc* mutants have physiological defects in stomatal function and plant growth that have not been described previously. These findings suggest that clathrin supports specific functions in multiple cell types. Stomata movement and gas exchange are altered in *chc* mutants, indicating that clathrin is important for stomatal regulation. The aberrant function of *chc* mutant stomata is consistent with the growth phenotypes observed under different water and light conditions, which also are similar to those of the secretory SNARE mutant, *syp121*. The *syp121* and *chc* mutants have impaired endocytosis and exocytosis compared with the wild type, indicating a link between SYP121-dependent secretion and clathrin-dependent endocytosis at the plasma membrane. Our findings provide evidence that clathrin and SYP121 functions are important for the coordination of endocytosis and exocytosis and have an impact on stomatal function, gas exchange, and vegetative growth in Arabidopsis (*Arabidopsis thaliana*).

Vesicle traffic to and from the plasma membrane plays an integral role in regulating protein localization and activity, membrane composition, and cell surface area. This traffic contributes to cell growth and development and to a wide range of physiological processes that enable plants to survive under varying environmental conditions. Exocytosis facilitates the distribution of proteins such as ion channels, receptors, and transporters to the cell surface at specific times and regions of the plasma membrane; it provides a mechanism for delivering cell wall components to the apoplast and supports cell growth and resistance to pathogens (Baluška et al., 2002; Sutter et al., 2007; Tyrrell et al., 2007; Bassham and Blatt, 2008). Vesicle fusion adds a new lipid bilayer to the plasma membrane that accommodates changes in cell shape and cell size (Battey et al., 1999; Geelen et al., 2002; Grefen et al., 2011). These fusion events are mediated by Soluble NSF Attachment Protein Receptor (SNARE) complexes that assemble from subunits present at both the plasma membrane and the surface of the docking vesicles (Rothman and Wieland, 1996; Sanderfoot et al., 2000; Grefen and Blatt, 2008). SNARE proteins are well conserved in eukaryotes, although in plants this family of proteins is greatly expanded, suggesting that vesicle traffic is either more complex or more abundant in comparison with the animal kingdom (Uemura et al., 2004; Sanderfoot, 2007; Honsbein et al., 2011).

Exocytic pathways to the plasma membrane are complemented by endocytic traffic that removes and recycles proteins and lipids from the plasma membrane, thereby regulating their presence and activity (Becker et al., 2003; Dhonukshe et al., 2007; Sutter et al., 2007; Kitakura et al., 2011). This other side of the traffic cycle at the plasma membrane is equally critical for physiology and development. The polarized localization of PIN proteins, for example, is maintained by the coordinated transport between the plasma membrane

www.plantphysiol.org/cgi/doi/10.1104/pp.17.00970

and endomembrane compartments to provide directional gradients of auxin in plants (Feraru and Friml, 2008; Kitakura et al., 2011; Jásik et al., 2013, 2016). When endocytosis is disrupted, this polarized expression is lost and auxin gradients dissipate (Kitakura et al., 2011). SNARE proteins localized on vesicles also must be returned to their originating, internal membranes after vesicle fusion, which requires endocytosis (Abeliovich et al., 1999; Enami et al., 2009). Indeed, although direct evidence is scant, there is a general agreement that both exocytic and endocytic pathways of the trafficking cycle at the plasma membrane are important for multiple plant cell functions and that the two processes must be tightly coordinated. Certainly, suppressing secretory traffic is known to have an impact on endocytosis (Battey et al., 1999; Geldner, 2004; Bandmann et al., 2011), but whether altered endocytosis affects exocytic traffic in many instances remains an open question.

Clathrin is a key structural protein that forms a lattice-like complex that includes two heavy chain subunits (CHC1 and CHC2) and two light chain subunits (CLC1 and CLC2). The subunits assemble a cage-like scaffold around developing vesicles to support vesicle formation at the plasma membrane and endosomal membranes in plants and animals (Goud et al., 1991; Blackbourn and Jackson, 1996; Puertollano et al., 2001; Holstein, 2002; Baisa et al., 2013). This scaffolding dissociates once the vesicle is fully formed and detached from the initial membrane by dynamin (Damke et al., 1994; Konopka et al., 2008), allowing the now naked vesicle to traffic to its destination. In plants, although a reduction in endocytosis has been noted in the roots of chc2 mutants, the known single chc mutant alleles do not present severe phenotypes, (Kitakura et al., 2011), suggesting a redundancy in function of the subunits. However, a tamoxifen-inducible dominant negative mutant line (HUB1) allows for the observation of the severe repercussions of the total loss of clathrin function. When induced, the dominant negative HUB1 mutant has stunted growth in multiple organs, indicating a requirement for clathrin function for the development of multiple cell types (Liu et al., 1995, 1998; Tahara et al., 2007; Robert et al., 2010). The endocytic and exocytic machinery are widely expressed in all cell types, and their functions, while similar, support the specialization of the different cell types that make up the organism. Therefore, all cells require both secretion and endocytosis for their growth and function. Clathrin is a major player in the regulation of endocytosis at the plasma membrane, but how its function relates to the coordination of vesicle traffic in plant cells is less defined.

Stomatal guard cells provide a particularly good example of the juxtaposition of exocytic and endocytic traffic in plants and our limited understanding of their coordination. Guard cells control transpiration by regulating the aperture of the stomatal pores in the leaf epidermis to facilitate gas exchange for photosynthesis while minimizing transpirational water loss. Guard cells undergo a 2- to 3-fold increase in cell volume and a 30% to 40% increase in surface area as the stoma opens,

and these processes are reversed as the guard cells close the stomatal pore (Blatt, 2000; Shope et al., 2003; Meckel et al., 2007; Bauer et al., 2013). Changes in cell volume are driven by solute uptake and loss, primarily of K^+ salts, and are regulated by a number of signals including changes in cytosol-free $[Ca^{2+}]$ (Blatt, 2000; Minguet-Parramona et al., 2016). Membrane traffic, including the traffic of K^+ channels, plays a key part in these events (Sutter et al., 2007; Eisenach et al., 2012). Furthermore, the block of exocytosis has been shown to suppress stomatal closure (Leyman et al., 1999), even though closure is commonly associated with endocytosis and the internalization of membrane material and proteins (Eisenach et al., 2012). In short, while all evidence supports a requirement for vesicle traffic in stomatal function, it is not clear how the two sides of the trafficking cycle to and from the guard cell plasma membrane are linked.

We asked how the clathrin machinery contributes to the coordination of plasma membrane traffic and cell function using chc1 and chc2 mutants. We also further characterized the hot ABA-deficiency suppressor1 (has1) mutation as a new CHC1 mutant allele (Plessis et al., 2011), which has a premature stop codon in the CHC1 gene in Arabidopsis (Arabidopsis thaliana). While clathrin functions at several internal membranes, the effect clathrin has on traffic is obvious at the plasma membrane, which can be readily monitored with the use of FM dyes in expanding root epidermal cells. Stomata of the has1 mutant are more closed under dehydration stress conditions (Plessis et al., 2011), indicating a new phenotype associated with the CHC1 mutant alleles and providing evidence for clathrin-mediated endocytosis in stomatal function. We further characterize the phenotypes of the chc1 and chc2 mutants and show that they are defective in both endocytosis and exocytosis, which, in turn, affects cellular functions and environmental response. We also show that the secretory syp121 mutant has a reduced rate of endocytosis, again supporting a mutual requirement for both arms of the trafficking cycle for productive vesicle transport at the plasma membrane. We further suggest that SYP121 and clathrin contribute to the coordination of vesicle transport at the plasma membrane and that disruption of this coordination can be observed in the defective stomatal behavior in the syp121 and chc mutants, which inhibits these mutants from quickly responding to their changing environments. The downstream effects of these molecular defects result in altered plant growth.

RESULTS

The has1 Mutation Is a New chc1 Allele in Arabidopsis

The has1 mutant was originally identified in an infrared imaging screen of a γ-ray mutagenized population of the ABA deficient3 (aba3-1) mutant. The has1 aba3-1 double mutation suppressed the cold-leaf phenotype associated with increased transpiration in the original aba3-1 mutant. Fine-mapping localized the has1 mutation

to a region on the lower arm of chromosome 3 between 2.1 and 3.7 Mb (Plessis et al., 2011). After backcrossing to the wild type Columbia-0 (Col-0) and segregation of the aba3-1 mutation, the has1 mutant was shown to have defects in stomatal responses to abscisic acid (ABA), which conferred a water stress-tolerant phenotype (Plessis et al., 2011). With further mapping, we reduced the interval to 0.4 Mb, and next-generation DNA sequencing of has1 identified a five-nucleotide deletion in the 23rd exon of the CHC1 gene (At3g11130) that introduces a frame shift and produces a premature stop codon into the CHC1 gene (Supplemental Fig. S1). To confirm the has1 mutant as a chc1 mutant, we included other chc1 mutant alleles and those of a close family member, CHC2, to explore their effects on secretion and the connection between clathrin-mediated endocytosis and plasma membrane transport. When gene-specific primers (Kitakura et al., 2011) were used with genomic DNA from wild type Col-0 and chc1-1, chc1-2, chc1-3, chc2-1, and chc2-3 mutants, PCR products could be amplified only from the wild-type template, while the products amplified using the T-DNA left border-specific primer with gene-specific primers were observed only in the mutant lines (Supplemental Fig. S1B). These results indicate that gene transcription in the chc mutants is completely disrupted and that each of the chc mutant alleles is a null mutant. There is no effective antibody specific to the CHC1 protein; therefore, we used RT-PCR and the same gene-specific primers to amplify cDNA products and confirm that gene transcripts are not present in these mutants (Supplemental Fig. S1C). These data are consistent with Kitakura et al. (2011) and again show that the mutant lines are null mutants in the CHC1 and CHC2 genes. These mutants are unlikely to produce a full-length protein product; therefore, we used at least one representative mutant for each CHC gene in the subsequent experiments.

The chc1 and chc2 Mutants Have Reduced Rates of Endocytosis

We compared the rates of endocytosis in the wild type (Col-0), chc1, chc2, has1, and induced HUB1 dominant negative mutant seedlings grown in liquid culture by measuring the internalization of the styryl dye FM4-64 over time in epidermal root cells using laser scanning confocal microscopy. The HUB1 lines express a truncated form of CHC1 under the control of a tamoxifen-inducible promoter. When the HUB1 fragment is expressed, it binds together with endogenous clathrin subunits to form a nonfunctional lattice that cannot produce a vesicle coat (Liu et al., 1995). Thus, expressing the HUB1 fragment effectively blocks all clathrin-mediated endocytosis. To induce the expression of the HUB1 fragment, seedlings were incubated with tamoxifen for 2 d prior to the experiment, and induction was confirmed by the observation of multiple severe growth defects (Supplemental Fig. S2). Our observations showed a slower rate of FM4-64 internalization in

the has1 and chc mutants compared with the wild type and the uninduced HUB1 line; the induced HUB1 line had almost no internalization of FM4-64 over the course of 30 min (Fig. 1). To quantify these results, we fitted the internal FM4-64 fluorescence signals to an exponential function to extract the time constants for its internalization. We approximated internalization using a single exponential function:

$$R_t = F_{int}/F_{per} = R_o + R_{max}\left(1-e^{-kt}\right) \qquad (1)$$

where R_t at time t is the ratio of fluorescence signals; F_{int} and F_{per} are the fluorescent signals measured inside the cell and at its perimeter, respectively; R_o is the initial fluorescence signal ratio or offset; R_{max} is the maximum amplitude of the fluorescence ratio; and k is the rate constant for internalization. Curve fittings were carried out jointly with data from the different lines while holding one or more of these parameters constant between data sets to minimize the number of free parameters. The best and visually satisfactory fittings were obtained when R_o and R_{max} were held constant and only k was allowed to vary between data sets. This analysis indicated that the rates of endocytosis were significantly slower in the has1, chc1-2, and chc2-1 mutant lines when compared with the wild type (Fig. 1B). These mutants each yielded an endocytic rate that was roughly 25% that of the wild-type control. Furthermore, when clathrin function was completely abolished in the induced HUB1 seedlings, endocytosis was greatly reduced to approximately 3% of wild-type endocytic rates (Table I). This analysis demonstrates the shared endocytic defect of has1 and chc mutants, consistent with has1 being an additional chc1 mutant allele. While it has already been shown that the chc2 mutant has reduced endocytosis (Kitakura et al., 2011), our data further illustrate that this also is observable in chc1 mutant alleles using our method and is due to a significant reduction in the rate of endocytosis rather than to a general loss of endocytic activity.

Secretion Is Inhibited by Defects in Clathrin-Mediated Endocytic Pathways

Given that the trafficking pathways to and from the plasma membrane are considered to rely on each other (Murphy et al., 2005; Tanaka et al., 2014), we asked if secretion was altered in the chc mutants using a transient expression assay in seedling roots. To visualize secretion in the chc mutants, seedling roots were transiently transformed with a single, multicistronic vector that allows for the expression of a secreted YFP (secYFP) protein, a retained GFP-HDEL protein, and a gene of interest. This vector enables the quantification of secretion using GFP-HDEL as a reference for ratiometric analysis and as a control for transformation (Karnik et al., 2013). Seedlings were transiently transformed with either the vector carrying secYFP and GFP-HDEL alone to visualize bulk secretion patterns in
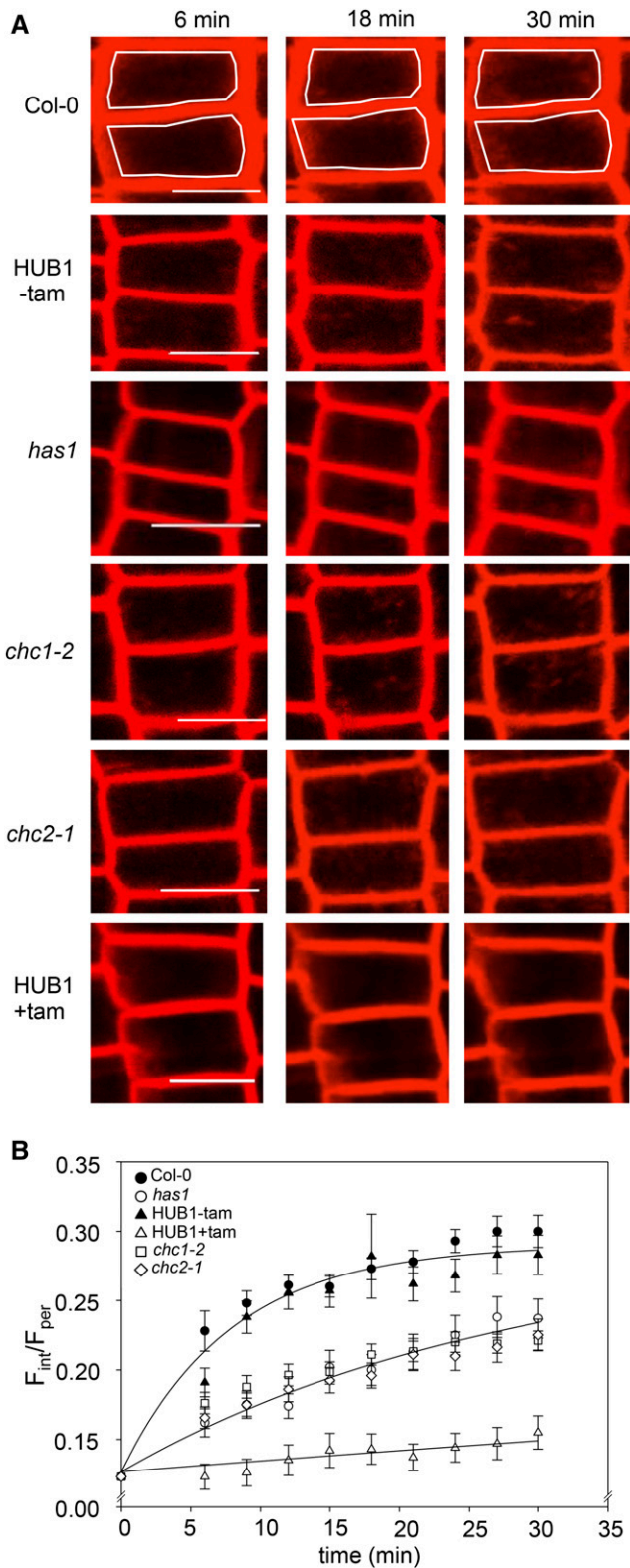
Figure 1. The rate of endocytosis is reduced in the *chc* mutant lines. A, Seedling roots were labeled with FM4-64 to measure internalization over time. The endocytosis rate was reduced in *has1* and other *chc1* alleles as well as in the *chc2* mutant compared with the wild type (Col-0) and the untreated HUB1 line (−tam). Almost no internalization is

the different genetic backgrounds or with the cytoplasmic fragment of the plasma membrane SNARE protein, SYP121 (SYP121$^{\Delta C}$), expressed in the third cassette as a positive control for secretion blockage (Karnik et al., 2013). When secretion occurs without blockage in transformed root epidermal cells, YFP fluorescence is lost as the secYFP protein diffuses out into the apoplast, leading to a low ratio of secYFP/GFP-HDEL fluorescence in the tissue. However, in the presence of secretory antagonists such as SYP121$^{\Delta C}$, the secYFP is trapped within the cells and the secYFP/GFP ratio increases (Grefen et al., 2015). When the secYFP/GFP-HDEL ratios were compared between the different genotypes, wild-type roots expressing SYP121$^{\Delta C}$ elicited a higher level of internal secYFP signal than when expressing secYFP and GFP-HDEL alone; however, the two independent *chc1* mutant alleles had a block in secretion regardless of the presence of SYP121$^{\Delta C}$ (Fig. 2). These data indicate that clathrin function affects secretion pathways to the plasma membrane as well as reduces the rate of endocytosis from the plasma membrane.

The reduction in both endocytosis and secretion in the *chc* mutants prompted us to ask if endocytosis is altered in a known secretory mutant. The Qa-SNARE, SYP121, is required for secretory pathways to the plasma membrane (Fasshauer et al., 1998; Geelen et al., 2002; Geldner, 2004; Enami et al., 2009), shown by a significant block of secretion in the *syp121* null mutant (Eisenach et al., 2012). We hypothesized that if secretion is altered by defects in clathrin endocytic machinery function, then endocytosis could be altered when secretory machinery function is compromised. We generated new FM4-64 internalization measurements to compare endocytic rates in Col-0 and *syp121*, *syp122*, *chc1-2*, and *chc2-1* mutant lines and calculated the half-time for each genotype. The internalization half-time of the FM6-64 dye in *syp121* mutants was greater than that in the wild type, indicating that endocytosis is reduced in the *syp121* secretory mutant as well as in the endocytic *chc* mutants compared with the wild type (Fig. 3; Table II). Endocytosis in the less severe secretion mutant *syp122* was not significantly affected. These data support a model for the link between the functions of molecular machinery that mediate both inward and outward patterns of vesicle transport.

observed in the HUB1 line pretreated with tamoxifen (+tam). The white frames in the Col-0 images highlight the boundary between the periphery (F_{per}) and internal spaces (F_{int}) of single cells that were used for fluorescence measurement. Bars = 10 μm. B, Graphical representation of FM4-64 internalization in Col-0, *chc* mutant lines, and the inducible dominant negative mutant HUB1 line treated with (+) and without (−) tamoxifen over time. Curves are joint fittings using Equation 1 with R_o and R_{max} held in common between data sets; the *y* axis is plotted as the ratio of fluorescence values (F_{int}/F_{per}) in reference to Equation 1. The *has1* and *chc* mutants show approximately 75% reduction in the rate of endocytosis, while endocytosis in the induced HUB1 seedlings was reduced to approximately 3% of the wild-type control. Values are means ± SE; *n* > 30 cells per genotype.

Table I. *Comparison of FM4-64 endocytosis rates in wild-type and chc mutant root epidermal cells*

Fitted rates for endocytosis are from the data of Figure 1B. Data were fitted jointly to Equation 1, with values for R_o and R_{max} held in common between data sets, yielding R_o of 0.134 ± 0.005 and R_{max} of 0.158 ± 0.006. Fittings to the individual mutant lines yielded statistically equivalent results.

Genotype	Endocytosis Rate (k)	k Relative to the Wild Type
	min^{-1}	
Wild type (Col-0), HUB −tam	0.118 ± 0.013	
has1, chc1-2, chc2-1	0.032 ± 0.003	0.27
HUB +tam	0.003 ± 0.002	0.02

The *chc1* Mutation Affects Stomatal Function

The stomatal defect reported in the *has1* mutant (Plessis et al., 2011) inspired us to investigate the stomatal activity in the other *chc* mutants in more detail. For these experiments, we applied exogenous Ca^{2+} to mimic ABA-triggered stomatal closure (Allen et al., 2001, 2002; Yang et al., 2006; Cho et al., 2009; Eisenach et al., 2012). We again used the HUB1 lines as an additional control for the *chc1* and *has1* mutant alleles. Epidermal peels were mounted in a custom perfusion chamber and incubated in a depolarizing buffer (DB; 0 mM Ca^{2+} and 60 mM K^+) to stimulate stomatal opening and then replaced with a hyperpolarizing buffer (HB; 6 mM Ca^{2+} and 0.1 mM K^+) to stimulate stomatal closing (Allen et al., 2001; Eisenach et al., 2012). The wild-type stomata closed in response to the HB and reopened with DB treatment over the 3 h of treatment (Fig. 4). The *has1* mutant stomata closed and reopened slower under these treatment conditions over the measured time period. After induction, the HUB1 line was unable to reopen after HB-induced stomatal closure. These data are similar to those seen in plants treated with the endosomal recycling inhibitor brefeldin A (BFA; Geldner et al., 2001; Nebenführ et al., 2002; Eisenach et al., 2012) and underscore the requirement for both endocytic and exocytic pathways in stomatal function, for which clathrin is required. We also measured the transpiration in whole plants to assess the stomatal dynamics of another *chc1* mutant allele in response to changing CO_2 levels (Fig. 4C). The results were consistent with the previous stomatal aperture measurements in *has1* and identify both a slower closing and reopening of stomata, which could contribute to the overall *chc1* mutant phenotype.

We hypothesized that the endocytosis defects observed in the roots of *chc1* mutants could represent a similar defect in stomata and contribute to their defective behavior. We infused leaves of Arabidopsis wild-type and mutant lines with FM4-64 and measured its internalization over time in guard cells using a similar methodology to that described for root epidermal cells. While FM dyes are reported to label endosomal

compartments in guard cells of *Vica faba* (Meckel et al., 2004), quantitative measurement of FM dye uptake for endocytic analysis in Arabidopsis guard cells is not frequently reported. We found that the vacuum infusion of fully expanded leaves provided the best images for assessing membrane and internal compartment labeling in Arabidopsis guard cells using a 40× objective under oil immersion. We again observed a significantly slower rate of internalization of FM4-64 in the *chc1* guard cells compared with the wild type, indicating that the reduction in endocytosis in the *chc1* mutants is not cell type specific and also correlates to the stomatal defect in the clathrin mutants (Fig. 4D; Table III).
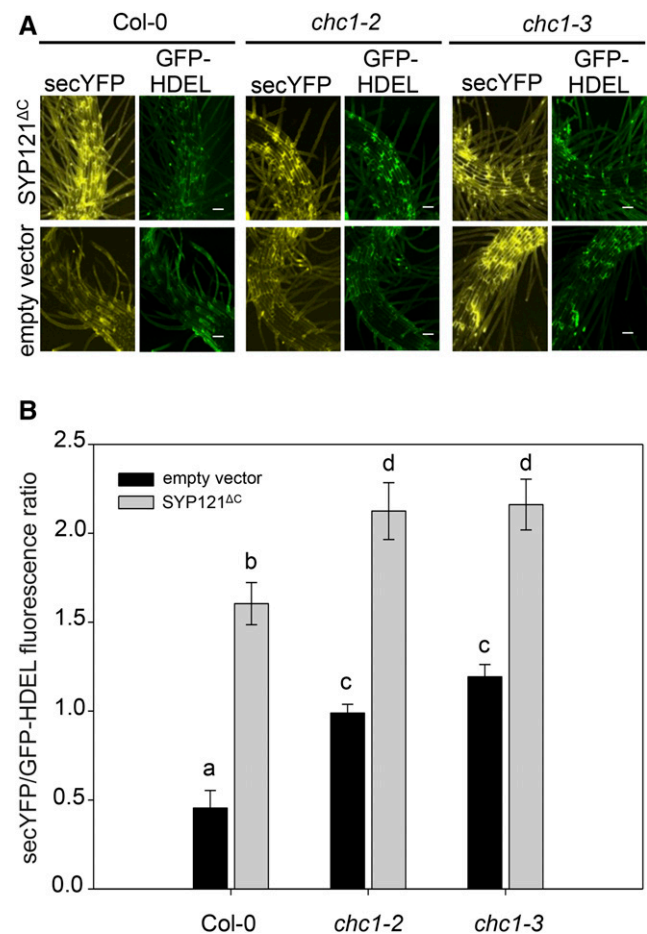

Figure 2. Secretion is inhibited in *chc1* mutants. A, The expression of a multicistronic vector expressing secYFP, GFP-HDEL, and the cytoplasmic fragment of the SNARE protein SYP121 (SYP121$^{\Delta C}$) inhibits secYFP secretion (top row) compared with the empty vector (bottom row). SYP121$^{\Delta C}$ blocks secretion in wild-type (Col-0) roots and enhances secretory blockage in the *chc1* mutants. Bars = 50 μm. B, Graphical representation of the fluorescence data presented in A. Letters indicate statistical significance by ANOVA, where $P < 0.005$ using the Holm-Sidak model. Values are means ± SE; $n > 6$ seedlings per genotype. Representative data from one of at least three independent experiments are shown.

Table II. *Comparison of FM4-64 endocytosis in wild-type and syp121 and syp122 root epidermal cells*

Fitted rates for endocytosis are from the data of Figure 3B. Data were fitted jointly to Equation 1, with values for R_o and R_{max} held in common between data sets, yielding R_o of 0.134 ± 0.005 and R_{max} of 0.159 ± 0.006. Fittings to the individual mutant lines yielded statistically equivalent results.

Genotype	Endocytosis Rate (k)	k Relative to the Wild Type
	min^{-1}	
Wild type (Col-0)	0.066 ± 0.009	
syp121	0.014 ± 0.002	0.21
syp122	0.043 ± 0.005	0.65
chc1-2	0.012 ± 0.002	0.18
chc2-1	0.011 ± 0.002	0.16

Loss of Clathrin Function Results in Growth Defects in *chc* Mutant Alleles

The *has1* mutant was initially identified in a thermoimaging screen of a mutant population and has stomata that are more closed under water stress (Plessis et al., 2011), consistent with the stomatal phenotype we describe for *chc1* mutants in this report (Fig. 4). Indeed, the *has1*, *chc1*, and *chc2* mutant alleles showed reduced water loss under rapid dehydration conditions when compared with wild-type plants (Fig. 5A). Thus, like the *has1* mutant, other *chc* mutants are more tolerant to water loss than wild-type plants.

We asked whether the dehydration-tolerant phenotype of the *chc* mutants might translate to changes in plant growth during longer periods of water stress in soil. Wild-type and *chc* mutant plants were grown in well-watered conditions for 3 weeks before all watering was stopped for 15 d and plant appearance was monitored. To quantify these differences, the ratio of the fresh and dry weights was determined from rosettes sampled from each line and used as an index for water loss. In plants subjected to dehydration, we expected the fresh weight-to-dry weight ratios to decrease; these ratios were significantly lower in the *chc1* and *chc2* mutants than in wild-type plants (Fig. 5B). These measurements are consistent with the visual appearance of *chc1* and *chc2* mutants, which had less visible wilting after 9 d of dehydration (Fig. 5C).

We also examined dehydration tolerance in two dominant negative HUB1 lines (Liu et al., 1995) to confirm the clathrin-dependent effect. This construct has been expressed successfully in plants to investigate the requirement for clathrin-mediated endocytosis in cell function (Tahara et al., 2007; Robert et al., 2010; Kitakura et al., 2011). For our experiments, all genotypes were treated with 2 μM tamoxifen for 2 d before watering was stopped, and parallel experiments without tamoxifen treatment were conducted as a control. When induced with tamoxifen, two independent HUB1 lines presented a dehydration-tolerant phenotype when compared to the wild type (Supplemental Fig. S3). All of the dehydration stress results are consistent

with the initial *has1* phenotype (Plessis et al., 2011) and show that the *chc* mutants lose less water over time compared to the wild-type plants. The HUB1 mutant further showed that near-complete inhibition of clathrin function provides a dehydration-tolerant phenotype and that clathrin function impacts water stress responses in plants.

The reduced vesicle transport, stomatal movement defects, and dehydration tolerance in *chc* mutants suggest that mutant plant growth could be affected under conditions that require tight stomatal regulation. Following germination, cohorts of wild-type, *has1*, *chc1*, and *chc2* plants were grown under combinations of 70 or 150 μmol m^{-2} s^{-1} light and 60% or 100% relative humidity (RH) in a short-day light regime for 2 weeks. When the mean rosette diameters were compared, the mutants were in most cases smaller than wild-type plants (Fig. 6). Under the control growth chamber settings (70 μmol m^{-2} s^{-1} light and 60% RH), the rosette diameters of the *chc* mutants were not significantly different from each other but were smaller than those of the wild type. No difference was observed between genotypes when plants were grown at elevated humidity (70 μmol m^{-2} s^{-1} light and 100% RH), suggesting that removing the pressure for water conservation masks the clathrin mutant growth phenotype. Indeed, when plants were grown in high light and reduced humidity conditions (150 μmol m^{-2} s^{-1} light and 60%
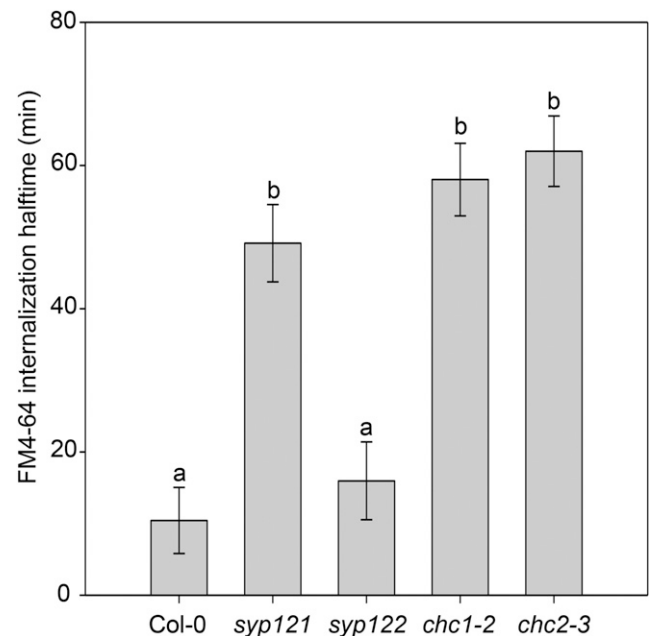

Figure 3. Endocytosis in *syp121* but not *syp122* mutants is slower than in the wild type, similar to the *chc* mutants. The half-times of FM4-64 internalization in the *syp* and *chc* mutants are greater than that measured in wild-type (Col-0) seedling roots. Letters indicate significant differences between genotypes from one of at least three independent experiments (ANOVA and the Holm-Sidak model, where $P = 0.001$); $n = 30$ cells measured across three seedlings per genotype.
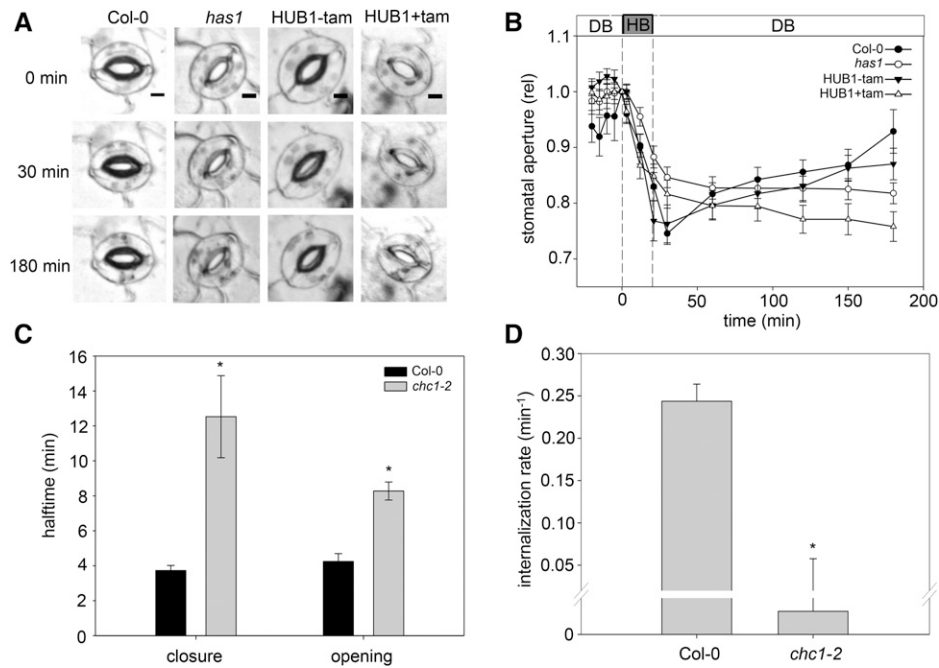
Figure 4. The reduced stomatal dynamics in the *chc1* mutant correlate with defects in endocytosis. A, Representative images of stomata during the hyperpolarizing (HB) and depolarizing (DB) buffer treatment time course in control (Col-0 and HUB1−tam) and experimental (*has1* and HUB1+tam) plants. Bars = 5 μm. B, Graphical representation of the change in stomatal aperture in response to HB or DB over time. The stomata of the *has1* mutant allele and induced HUB1 lines do not reopen after closure. These data represent three independent experiments consisting of at least 24 individual stomata per genotype and are means ± SE. C, The half-times for stomatal closure and opening in Col-0 and *chc1* mutant plants were calculated from transpiration measured during a CO_2 treatment sequence (2 h at 400 μL L^{-1}, 2 h at 1,000 μL L^{-1}, and 3 h at 400 μL L^{-1}). Asterisks indicate significant differences from the wild type (Student's *t* test, where $P < 0.005$). Values are means ± SE; $n = 5$. D, FM4-64 internalization rates in Col-0 and *chc1* guard cells. A ratio of the internal-to-peripheral FM4-64 signals was calculated, and the initial value was subtracted from each subsequent value to offset the data. The internalization rates were then calculated. Values are means ± SE; data from four to eight guard cells from independent plants for each genotype are presented. The asterisk indicates a significant difference from the wild type (Student's *t* test, where $P < 0.001$).

RH), which impose a requirement for water conservation in addition to high photosynthetic activity, the mutant plants were significantly smaller than wild-type plants. Interestingly, the *chc2* mutants also were significantly smaller than the *chc1* mutants under these conditions, suggesting a potential divergence in CHC1 and CHC2 functions. We measured steady-state transpiration in wild-type, *chc1*, and *chc2* plants and observed lower transpiration levels in the clathrin mutant lines (Fig. 6C), which is consistent with stomata that are, in general, more often closed. Altogether, these data underscore the requirement for clathrin function during plant growth under conditions that increase photosynthetic activity and require well-regulated stomatal movements.

DISCUSSION

The impact of secretory inhibition on cell function is well documented, and several reports show that prolonged inhibition of secretory pathways ultimately affects endocytosis (Geldner et al., 2001; Nebenführ et al.,

2002; Richter et al., 2007). These reports, however, are based mainly on studies with inhibitors like BFA that broadly affect traffic through the Golgi and the trans-Golgi network, which serves as a hub for both endocytic and exocytic trafficking pathways in plants. Thus, a clear delineation and assessment of the direct effects of one pathway alone are difficult to elucidate. Using genetic mutants allowed us to observe the effects of a direct loss of clathrin mechanical function during vesicle transport. With the genetic and physiological tools

Table III. *Comparison of FM4-64 endocytosis rates in wild-type and chc1 mutant stomata*

Internalization rates for endocytosis are from the data of Figure 4D. Analysis is shown for data ± SE from at least five to eight stomata per genotype using a single exponential function (SigmaPlot version 11.0).

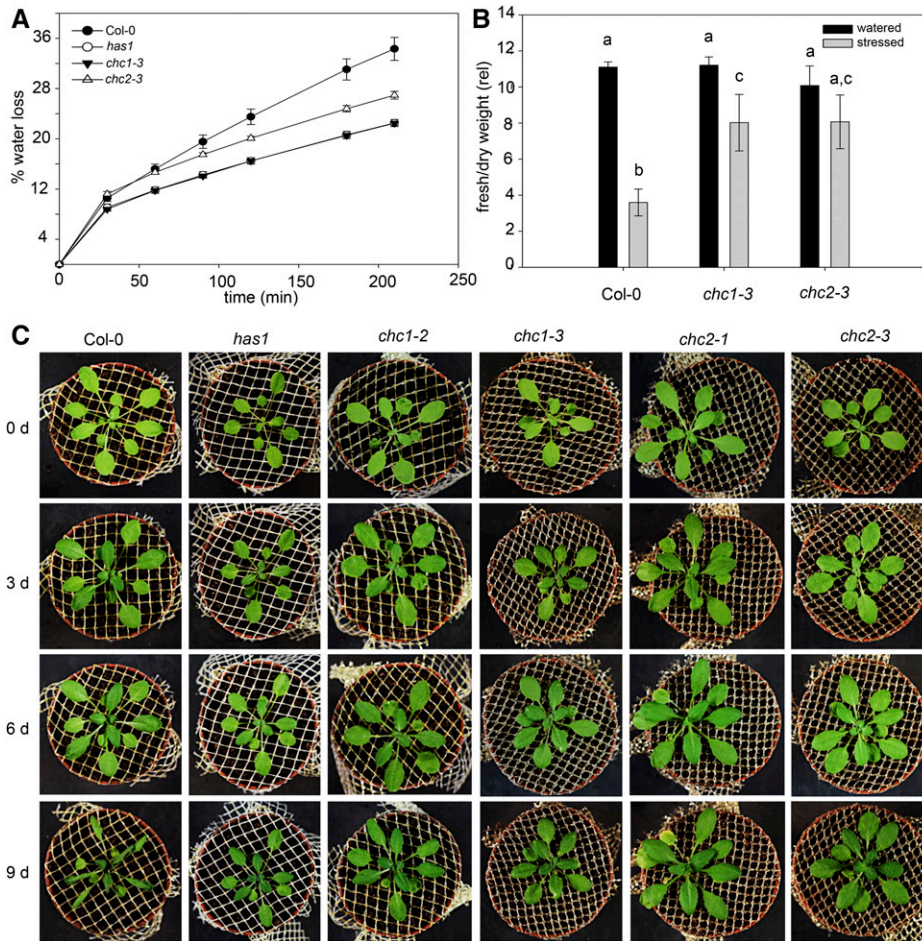| Genotype	Endocytosis Rate (k)	k Relative to the Wild Type
	min^{-1}	
Wild type (Col-0)	0.24 ± 0.02	
chc1-2	6.3×10^{-5} ± 0.04	0.26×10^{-3}

Figure 5. The *chc* mutants are more tolerant to water loss than wild-type Arabidopsis. A, The *has1*, *chc1*, and *chc2* mutants are more tolerant to rapid dehydration compared with wild-type (Col-0) plants, indicated by a lower percentage of water loss. Values are means ± SE; $n = 4$. B, Water loss is reduced under longer dehydration conditions in the *chc* mutants compared with wild-type plants, as shown by the mean fresh weight-to-dry weight ratios from 15-d-old rosettes. Values are means ± SE; $n = 10$ plants for each genotype. Letters indicate significance calculated from ANOVA, where $P < 0.005$ (Holm-Sidak). C, Representative images of plants from each genotype after 0, 3, 6, and 9 d of no watering ($n = 5$). Results are from one of three independent experiments.

available in plants, we can now show (1) that disruption of either exocytic or endocytic pathways in stomata as well as other cell types leads to physiological consequences, evident in the suppressed growth and enhanced dehydration resistance of the *chc* mutants; (2) that endocytosis and exocytosis are essential for stomatal function; and (3) that, where secretion is impaired in the clathrin mutants, endocytosis is impaired in the *syp121* mutant, indicating that these pathways are linked in their function and in their effects on cell function and plant physiology.

Endocytosis and Exocytosis Are Linked Pathways That Can Mutually Affect Each Other

While endocytosis was examined previously in *chc1* and *chc2* mutants (Kitakura et al., 2011), the rates of this traffic have not been measured directly in order to link the consequences of the reduction in endocytosis to a physiological behavior. We found that single mutations in *CHC1* or *CHC2* decrease the rate of endocytosis, increasing the half-time for FM4-64 internalization by roughly 4-fold compared with that of wild-type cells (Fig. 1). Kitakura et al. (2011) also used FM4-64 internalization to assay endocytosis in *chc* mutants

and end-point measurements after 6 min, an approach that did not detect differences in endocytic rates that are evident with a multiple measurement time-course experiment. Thus, our endocytic rate analysis is consistent with their end-point results, improves the characterization of *chc1* endocytic defects, and highlights the importance of a kinetic analysis of vesicle traffic in these circumstances. The results from the single *chc1* and *chc2* mutants indicate that a partial block in clathrin function has a negative impact on plant cell growth and regulation. This requirement for clathrin-dependent vesicle traffic for plant cell growth may not be surprising when considered with the role that clathrin plays in auxin efflux and plant development (Tahara et al., 2007; Wang et al., 2013; Yu et al., 2016).

Current models of the relationship between endocytosis and exocytosis are based primarily on experiments with BFA and suggest that an extended block of exocytosis leads to the accumulation of vesicles from endocytic pathways within so-called BFA compartments. The BFA sensitivity of these pathways is related to ARF-GEF protein inhibition and the consequences for the associated GTPases (Nebenführ et al., 2002; Geldner, 2004; Richter et al., 2007; Teh and Moore, 2007; Robinson et al., 2008). In both cases, these ARF-GEFs
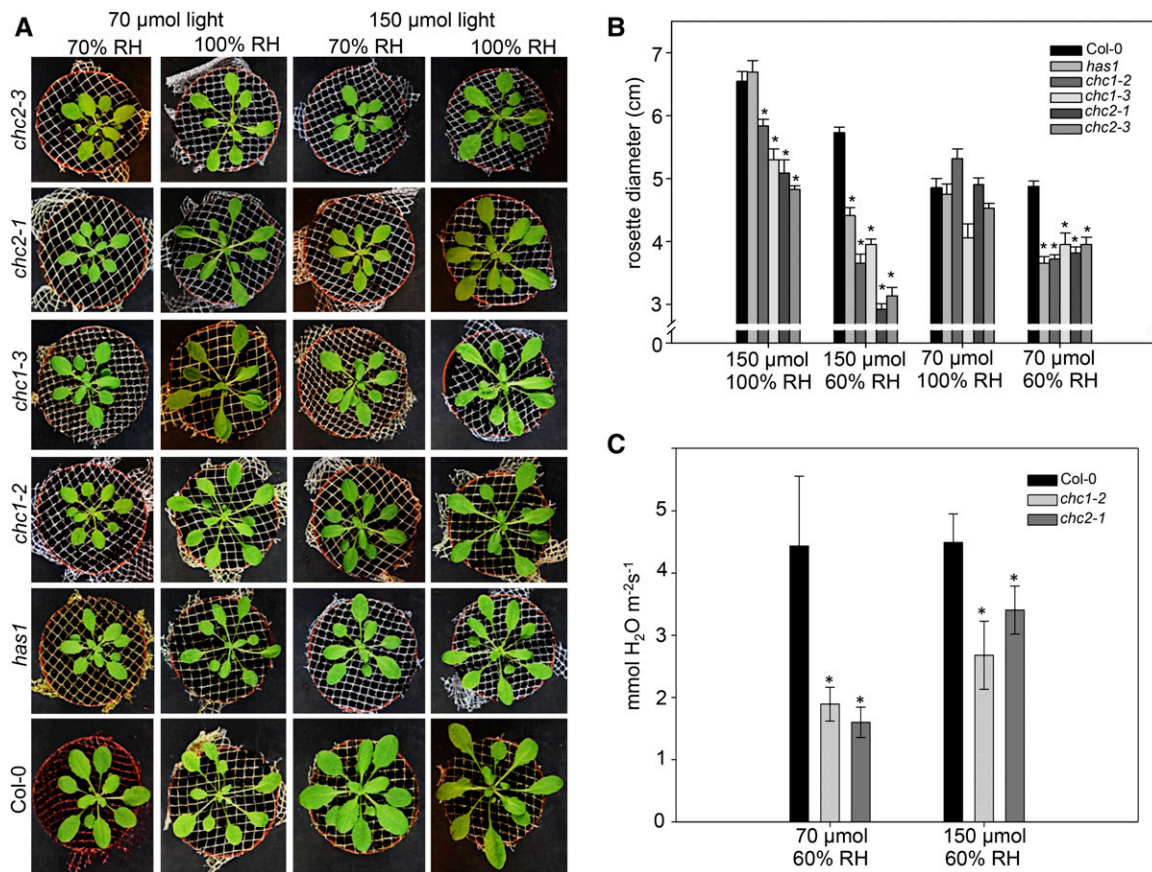
Figure 6. *chc1* and *chc2* mutants are sensitive to changes in light and humidity due to defective stomatal function. A, Representative plants grown under control light (70 μmol m^{-1} s^{-1}) or high light (150 μmol m^{-1} s^{-1}) and control RH (60%) or high RH (100%). The mutant rosettes are smaller in lower RH conditions, particularly when in high light. The growth phenotype is rescued under high humidity and control light conditions. B, Graphical representation of mean rosette diameter for each genotype under the different growth conditions. C, Steady-state transpiration rates (mmol water m^{-2} s^{-1}) in the *chc* mutant plants are lower than that of Col-0 in control and high-light conditions. In both B and C, asterisks indicate significant differences from the wild type in each condition (Student's *t* test, where $P < 0.005$). Values are means $\pm$ SE; $n = 4$ plants in each experiment, which was conducted three times.

serve as regulators of trafficking pathways and associate with endosomal compartments that are integral to recycling patterns at the plasma membrane (Geldner, 2004); thus, they target the junctions between endocytic and exocytic processes. In contrast, we show here through direct mutation of the clathrin machinery that traffic to the plasma membrane is impaired when the major regulator of endocytosis at the plasma membrane is compromised (Fig. 2). Furthermore, the stark phenotypic similarities between the *syp121* and *chc* mutants are genetic indicators of a mutual functional dependency between endocytic and exocytic mechanisms (Figs. 2, 3, and 6). These findings provide clear evidence of the link between the secretory and endocytic pathways at the plasma membrane.

Clathrin Is Essential for Stomatal Function

Our findings connect clathrin function to stomatal behavior in a manner that is counterintuitive. Through the identification of the *has1* mutant as a new *chc1* mutant allele, we show that *chc1* mutant plants have stomata that are impaired in their closure as well as reopening, indicating a requirement for clathrin-mediated transport in guard cell function (Fig. 4). While the *chc1* stomata can open, their defective movement indicates a misregulation that has physiological effects on the plant, seen in the dehydration tolerance phenotype in both the *chc1* and *chc2* mutants: stomata of these mutants can close in response to dehydration stress signals, but they remain closed for longer periods of time when compared with the wild type. This defective stomatal movement leads to an increase in water retention under water-deficient conditions, which is most easily explained by the impaired ability of *chc* mutants to reopen after stomatal closure. Our further analysis of gas exchange in the *chc1* mutants, which have lower transpiration levels compared with wild-type plants, again corresponds to a defect in stomatal aperture regulation (Fig. 4).

Such impairment in reopening is surprising because opening is normally associated with exocytic traffic as the guard cell expands and its surface area increases. Indeed, these observations parallel those in the SNARE mutant, *syp121*, which also fails to reopen the stomata after Ca^{2+}-induced closure (Eisenach et al., 2012). Our findings also juxtapose earlier observations that the dominant negative SYP121$^{\Delta C}$ fragment interferes with K^+ channel regulation and stomatal closure (Leyman et al., 1999; Sokolovski et al., 2008), although SYP121$^{\Delta C}$ acts primarily by blocking exocytosis (Geelen et al., 2002; Tyrrell et al., 2007; Grefen et al., 2015; Karnik et al., 2015). Our secretion analysis in *chc* and *syp121* mutants shows that both endocytosis and exocytosis are impaired (Figs. 1–3). These results demonstrate a dependence on both secretion and endocytosis in stomatal opening as well as closing, highlighting the close coordination between the two sides of the trafficking cycle; indeed, the reduced endocytosis we measured in *chc1* mutant guard cells confirms that vesicle traffic at the plasma membrane in these cells is compromised and contributes to the mutant phenotype (Fig. 4D). We cannot rule out the function of clathrin at other endomembrane compartments that also are involved in cell growth and function, and certainly secretion could be affected by the inhibition of clathrin-mediated vesicle formation at the Golgi or the trans-Golgi network (Puertollano et al., 2001); however, our results clearly show the effects that the *chc* single mutants have on vesicle traffic at the plasma membrane. Furthermore, the juxtaposition of the *syp121* mutant phenotypes suggests that the block of secretion we observed in *chc* mutant plants is potentially an immediate effect of the clathrin mutations on vesicle traffic at the plasma membrane (Figs. 1–4). During stomatal opening, the requirement for both secretion and endocytosis to regulate cell expansion may exacerbate the mutant phenotype, presenting the effects we observed in stomatal reopening, transpiration, and plant growth. Further experimentation will focus on stomatal conductance kinetics and in exploring the nuance of vesicle trafficking during guard cell dynamics.

Physiological Consequences of Defective CHC Function

The dehydration-tolerant phenotype observed in each of the *chc1* and *chc2* mutant alleles (Fig. 5) is consistent with previous findings that the *chc1* mutants close their stomata in response to low concentrations of exogenous ABA (Plessis et al., 2011). These observations indicate that the plants either are better able to sense water loss or are deficient in their ability to closely regulate transpiration compared with wild-type plants. The *chc* mutant plants are smaller under our growing conditions compared with the wild type and are substantially smaller still when grown under high light and lower humidity (Figs. 5 and 6). Much like what has been demonstrated in the *syp121* mutant, this reduction in growth is most likely the result of reduced photosynthetic

activity due to the disrupted gas exchange/water regulation in the mutants, consistent with the reduced transpiration rates we observed (Fig. 6C). The growth phenotypes under these different water-stress conditions correlate well with the stomatal phenotype we observed in the *chc* mutants and mirror those of the *syp121* mutant (Eisenach et al., 2012). Again, the similarities between the growth phenotypes of the endocytic (*chc*) and exocytic (*syp121*) mutants suggest common underpinning mechanisms behind their physiological functions. Together with the inhibited secretion in the *chc* mutants, we now have cellular and genetic evidence for a coupling of the SNARE and clathrin machinery that are major players in vesicle transport at the plasma membrane. This coupling is vital for effective stomatal function and has major downstream effects on plant development.

MATERIALS AND METHODS

Plant Material and Growth Conditions

Seeds were surface sterilized with 20% sodium hypochlorite for 20 min at room temperature and then washed five to six times in sterile water. Seeds were then stratified in the dark for 48 h at 4°C before use. Arabidopsis (*Arabidopsis thaliana*) mutants *chc1-1* (SALK_112213), *chc1-2* (SALK_103252), *chc1-3* (SALK_018351), *chc2-1* (SALK_028826), and *chc2-3* (SALK_151638) in the Col-0 ecotype background were compared with the untransformed wild type (Col-0) in all experiments. After backcrossing to the wild type and segregation of the *aba3-1* mutation, the *has1* mutant was backcrossed twice to the wild type before analysis of mutant phenotypes.

Map-Based Cloning and Sequencing

For mapping, the leaf temperature of F2 progeny from crosses between *aba3-11* and *has1 aba3-1* was analyzed by thermal imaging, and DNA was extracted in a 96-tube format. The mapping interval was then determined after genotyping F2 plants using simple sequence length polymorphism markers, as described by Plessis et al. (2011). Genome sequencing was carried out on the *has1 aba3-1* mutant after two backcrosses to the *aba3-1* mutant. DNA was isolated as described by Sechet et al. (2015), and sequencing was performed by TGAC using an Illumina HiSeq 2000 sequencer.

Water Stress Experiments

Rapid dehydration assays were carried out using 3-week-old plants grown in the glasshouse (18°C–28°C, minimum 13-h photoperiod). Four rosettes per genotype were cut from the root system, placed abaxial face up on a support of absorbent paper and aluminum foil, and weighed before being placed in a lamina flow hood at ambient temperature. Plants were subsequently weighed at regular intervals to determine the rate of water loss (North et al., 2005). For phenotypic analysis of *chc* mutants under drought conditions, plants were grown on soil under 10 h of light/14 h of dark (150 μmol m^{-2} s^{-1}) at 18°C to 22°C. For each genotype, eight plants were watered every other day with 20 mL of water for 2 weeks, after which watering for four plants from each genotype was stopped for 12 d. Watering was continued for the other four plants from each genotype (Plessis et al., 2011). Images were taken every day after watering was stopped for the drought cohort, and on day 12, rosettes were collected and the fresh weight was measured. The rosettes were dried for 3 d at 60°C, and the dry weight of each was recorded.

Light and Humidity Growth Conditions

Single plants were grown from seeds in 6-cm pots and watered with tap water regularly for 3 weeks under either 70 or 150 μmol m^{-2} s^{-1} light intensity in short-day conditions (8 h of light/16 h of dark). In each of these light conditions, plants were either covered with a plastic dome to give greater than 98% RH or left uncovered (60% RH). Plants were imaged 20 d after germination.

Stomatal Aperture Measurements

Epidermal peels were mounted in a custom flow chamber and preincubated for 2 h in DB (10 mM MES-NaOH, pH 6.15, and 60 mM KCl). Sets of individual stomata were imaged throughout with continuous superfusion using a Leica SMD SP8 confocal microscope (Leica Microsystems). To induce stomatal closure, peels were treated with HB (10 mM MES-NaOH, pH 6.15, 0.1 mM KCl, and 6 mM CaCl$_2$) for 20 min. To induce reopening of stomata, DB was introduced into the chamber to replace the HB. Stomatal apertures were analyzed from three independent experiments (n = 22–30 stomata per genotype) using ImageJ version 1.48p (www.ImageJ.org). Chloroplast movement was used to confirm that living stomata were measured. Apertures were normalized on a cell-by-cell basis to measurements taken at the end of the preincubation period.

Genotypic Analysis

To isolate genomic DNA, 5- to 10-d-old seedlings grown in liquid 0.05× Murashige and Skoog (MS) medium were collected in 2-mL Eppendorf tubes, flash frozen on liquid nitrogen, and ground to a powder. A volume of 500 μL of extraction buffer (0.2 M Tris-HCl, pH 8, 0.4 M LiCl, 1% SDS, and 25 mM EDTA, pH 8) was added to each sample and mixed by vortexing. Samples were centrifuged at maximum speed for 10 min, and the supernatant was transferred to clean 2-mL tubes. Isopropanol was added to each tube at twice the sample volume and gently mixed by inversion, incubated at room temperature for 1 h, and centrifuged at 25,000g for 10 min. Supernatants were decanted, and the pelleted genomic DNA was allowed to dry before being resuspended in 50 μL of sterile water for use as PCR templates.

RNA was isolated from 5- to 10-d-old seedlings grown in liquid 0.05× MS medium using the RNeasy Mini-Kit for plants (Qiagen). To produce cDNA templates for RT-PCR, this RNA was used in the QuantiTect RT cDNA Synthesis Kit (Qiagen), following the manufacturer's instructions. Gene-specific primers to identify the mutant alleles of *chc1* and *chc2* (Kitakura et al., 2011) were used for genomic and RT-PCR amplification. KOD Hot-Start DNA polymerase was used according to the manufacturer's instructions (Merck Millipore). Volumes of 10 to 20 μL of the products were resolved on a 1.5% agarose gel.

FM4-64 Labeling and Endocytosis Measurements

Endocytosis rates were measured in Col-0, *has1* and *chc* mutants, and two HUB1-inducible lines grown with and without 2 μM tamoxifen to induce expression. Seedlings were stained for 1 min with 10 μM FM4-64 at 20°C. After FM4-64 washout, dye internalization was imaged over the course of 30 min using a Leica SMD SP8 confocal microscope (Leica Microsystems). FM4-64 signal was excited using the 488-nm laser line, and emission was detected over 620 to 780 nm after monochromatic beam splitting. Internalization was calculated per cell (n > 30 per genotype) as the ratio of the internal and plasma membrane signals, the latter defined as a 1-μm depth within the perimeter determined from bright-field images of the cell wall border. Rates for internalization were calculated from joint fittings to an exponential function (Eq. 1), with best fitting obtained assuming a common value for R_{max} between genotypes. In every case, internalization rates were compared by ANOVA with data from at least three independent experiments.

For FM4-64 measurements in guard cells, leaves from 3- to 4-week-old plants grown under short-day light conditions were vacuum infiltrated with 20 μM FM4-64 at room temperature (20°C) using a 10-mL syringe. Leaves were immediately mounted on slides for imaging. Stomata were imaged with a 40× objective; images were taken every 3 to 5 min for a total of 30 min. FM4-64 internalization was measured using the same technique described for root epidermal cells. A ratio of the internal-to-external fluorescence values was used to calculate the rate of internalization from pooled data from three to six stomata per genotype. More than five regions of interest from each time point were used in the internalization calculations. Error bars in the figures represent SE. Rates of internalization were calculated from the single exponential function in SigmaPlot version 11.0 (Systat Software). In every case, internalization rates were compared by ANOVA with data from at least four independent stomata.

Analysis of Secretion in Roots

Sterilized and stratified seeds were sown into 1 mL of 0.05× MS medium on 12-well plates. Transient transformations were carried out with the pTecG-2in1

vector (Karnik et al., 2013) following the protocol of Grefen et al. (2015). The inoculation solutions were added to the appropriate wells containing 3-d-old seedlings, and roots were imaged 3 to 4 d after coincubation. The GFP and YFP fluorophores were excited using 440- and 514-nm laser lines, respectively. After chromatic separation, GFP fluorescence was collected over 475 to 520 nm and YFP fluorescence was collected over 535 to 600 nm. Fluorescence images were rendered as 3D projections, and quantification of fluorescence intensities from the roots was calculated after subtracting the mean background fluorescence collected from similarly rendered projections of untransformed seedlings grown in parallel in each experiment (Karnik et al., 2013).

Steady-State Whole-Plant Transpiration Measurements

Wild-type and mutant Arabidopsis plants were grown on soil for 3 weeks under 70 or 150 μmol m^{-2} s^{-1} light in short-day conditions at 60% RH and 22°C. Using an LI-6400XT portable photosynthesis system (LI-COR Biosciences), measurements were collected every 10 s for 3 min using the whole-plant chamber to maintain the light, humidity, and temperature conditions in which each plant had been grown. Five plants of each genotype were measured, and mean values for the transpiration rates ± SE (mmol water m^{-2} s^{-1}) were plotted for each light condition.

Statistics

All data are reported as means ± SE of n independent experiments unless noted otherwise. ANOVA and Student's t test were carried out using SigmaPlot version 11.0 (Systat Software).

Accession Numbers

Accession numbers are as follows. For *CHC1* (At3g11130) and associated T-DNA mutants: *chc1-1* (SALK_112213), *chc1-2* (SALK_103252), and *chc1-3* (SALK_018351); for CHC2 (At3g08530) and associated T-DNA mutants: *chc2-1* (SALK_028826) and *chc2-3* (SALK_151638); *SYP121* (At3g11820) and the mutant *syp121-1* (*syr1/pen1-1*) is a point mutation mutant with a premature stop codon in the open reading frame (Leyman et al., 1999; Collins et al., 2003; Sokolovski et al., 2008); for *SYP122* (At3g52400) and the associated T-DNA mutant *syp122* (SALK_021525).

Supplemental Data

The following supplemental materials are available.

Supplemental Figure S1. Genotyping *chc1* and *chc2* mutant alleles.

Supplemental Figure S2. Tamoxifen treatment alters growth and root cell organization only in the HUB1 lines.

Supplemental Figure S3. Dehydration tolerance in two dominant negative HUB1 clathrin mutants.

LITERATURE CITED

Abeliovich H, Darsow T, Emr SD (1999) Cytoplasm to vacuole trafficking of aminopeptidase I requires a t-SNARE-Sec1p complex composed of Tlg2p and Vps45p. EMBO J **18:** 6005–6016

Allen GJ, Chu SP, Harrington CL, Schumacher K, Hoffmann T, Tang YY, Grill E, Schroeder JI (2001) A defined range of guard cell calcium oscillation parameters encodes stomatal movements. Nature **411:** 1053–1057

Allen GJ, Murata Y, Chu SP, Nafisi M, Schroeder JI (2002) Hypersensitivity of abscisic acid-induced cytosolic calcium increases in the *Arabidopsis* farnesyltransferase mutant *era1-2*. Plant Cell **14:** 1649–1662

Baisa GA, Mayers JR, Bednarek SY (2013) Budding and braking news about clathrin-mediated endocytosis. Curr Opin Plant Biol **16:** 718–725

Baluška F, Hlavacka A, Šamaj J, Palme K, Robinson DG, Matoh T, McCurdy DW, Menzel D, Volkmann D (2002) F-actin-dependent endocytosis of cell wall pectins in meristematic root cells: insights from brefeldin A-induced compartments. Plant Physiol **130:** 422–431

Bandmann V, Kreft M, Homann U (2011) Modes of exocytotic and endocytotic events in tobacco BY-2 protoplasts. Mol Plant **4:** 241–251

Bassham DC, Blatt MR (2008) SNAREs: cogs and coordinators in signaling and development. Plant Physiol **147:** 1504–1515

Battey NH, James NC, Greenland AJ, Brownlee C (1999) Exocytosis and endocytosis. Plant Cell **11:** 643–660

Bauer H, Ache P, Wohlfart F, Al-Rasheid KAS, Sonnewald S, Sonnewald U, Kneitz S, Hetherington AM, Hedrich R (2013) How do stomata sense reductions in atmospheric relative humidity? Mol Plant **6:** 1703–1706

Becker D, Hoth S, Ache P, Wenkel S, Roelfsema MRG, Meyerhoff O, Hartung W, Hedrich R (2003) Regulation of the ABA-sensitive Arabidopsis potassium channel gene GORK in response to water stress. FEBS Lett **554:** 119–126

Blackbourn HD, Jackson AP (1996) Plant clathrin heavy chain: sequence analysis and restricted localisation in growing pollen tubes. J Cell Sci **109:** 777–786

Blatt MR (2000) Cellular signaling and volume control in stomatal movements in plants. Annu Rev Cell Dev Biol **16:** 221–241

Cho D, Kim SA, Murata Y, Lee S, Jae SK, Nam HG, Kwak JM (2009) Deregulated expression of the plant glutamate receptor homolog AtGLR3.1 impairs long-term Ca^{2+}-programmed stomatal closure. Plant J **58:** 437–449

Collins NC, Thordal-Christensen H, Lipka V, Bau S, Kombrink E, Qiu JL, Hückelhoven R, Stein M, Freialdenhoven A, Somerville SC, et al (2003) SNARE-protein-mediated disease resistance at the plant cell wall. Nature **425:** 973–977

Damke H, Baba T, Warnock DE, Schmid SL (1994) Induction of mutant dynamin specifically blocks endocytic coated vesicle formation. J Cell Biol **127:** 915–934

Dhonukshe P, Aniento F, Hwang I, Robinson DG, Mravec J, Stierhof YD, Friml J (2007) Clathrin-mediated constitutive endocytosis of PIN auxin efflux carriers in Arabidopsis. Curr Biol **17:** 520–527

Eisenach C, Chen ZH, Grefen C, Blatt MR (2012) The trafficking protein SYP121 of Arabidopsis connects programmed stomatal closure and K^+ channel activity with vegetative growth. Plant J **69:** 241–251

Enami K, Ichikawa M, Uemura T, Kutsuna N, Hasezawa S, Nakagawa T, Nakano A, Sato MH (2009) Differential expression control and polarized distribution of plasma membrane-resident SYP1 SNAREs in *Arabidopsis thaliana*. Plant Cell Physiol **50:** 280–289

Fasshauer D, Sutton RB, Brunger AT, Jahn R (1998) Conserved structural features of the synaptic fusion complex: SNARE proteins reclassified as Q- and R-SNAREs. Proc Natl Acad Sci USA **95:** 15781–15786

Feraru E, Friml J (2008) PIN polar targeting. Plant Physiol **147:** 1553–1559

Geelen D, Leyman B, Batoko H, Di Sansebastiano GP, Moore I, Blatt MR (2002) The abscisic acid-related SNARE homolog NtSyr1 contributes to secretion and growth: evidence from competition with its cytosolic domain. Plant Cell **14:** 387–406

Geldner N (2004) The plant endosomal system: its structure and role in signal transduction and plant development. Planta **219:** 547–560

Geldner N, Friml J, Stierhof YD, Jürgens G, Palme K (2001) Auxin transport inhibitors block PIN1 cycling and vesicle trafficking. Nature **413:** 425–428

Goud B, Faivre-Bauman A, Picart R, Tixier-Vidal A (1991) Subcellular distribution of clathrin in cultured hypothalamic neurons. Biol Cell **72:** 83–92

Grefen C, Blatt MR (2008) SNAREs: molecular governors in signalling and development. Curr Opin Plant Biol **11:** 600–609

Grefen C, Honsbein A, Blatt MR (2011) Ion transport, membrane traffic and cellular volume control. Curr Opin Plant Biol **14:** 332–339

Grefen C, Karnik R, Larson E, Lefoulon C, Wang Y, Waghmare S, Zhang B, Hills A, Blatt MR (2015) Nat Plants **1:** 15166

Holstein SEH (2002) Clathrin and plant endocytosis. Traffic **3:** 614–620

Honsbein A, Blatt MR, Grefen C (2011) A molecular framework for coupling cellular volume and osmotic solute transport control. J Exp Bot **62:** 2363–2370

Jásik J, Boggetti B, Baluška F, Volkmann D, Gensch T, Rutten T, Altmann T, Schmelzer E (2013) PIN2 turnover in Arabidopsis root epidermal cells explored by the photoconvertible protein Dendra2. PLoS One **8:** e61403

Jásik J, Bokor B, Stuchlík S, Mičieta K, Turňa J, Schmelzer E (2016) Effects of auxins on PIN-FORMED2 (PIN2) dynamics are not mediated by inhibiting PIN2 endocytosis. Plant Physiol **172:** 1019–1031

Karnik R, Grefen C, Bayne R, Honsbein A, Köhler T, Kioumourtzoglou D, Williams M, Bryant NJ, Blatt MR (2013) *Arabidopsis* Sec1/Munc18 protein SEC11 is a competitive and dynamic modulator of SNARE binding and SYP121-dependent vesicle traffic. Plant Cell **25:** 1368–1382

Karnik R, Zhang B, Waghmare S, Aderhold C, Grefen C, Blatt MR (2015) Binding of SEC11 indicates its role in SNARE recycling after vesicle fusion and identifies two pathways for vesicular traffic to the plasma membrane. Plant Cell **27:** 675–694

Kitakura S, Vanneste S, Robert S, Löfke C, Teichmann T, Tanaka H, Friml J (2011) Clathrin mediates endocytosis and polar distribution of PIN auxin transporters in Arabidopsis. Plant Cell **23:** 1920–1931

Konopka CA, Backues SK, Bednarek SY (2008) Dynamics of *Arabidopsis* dynamin-related protein 1C and a clathrin light chain at the plasma membrane. Plant Cell **20:** 1363–1380

Leyman B, Geelen D, Quintero FJ, Blatt MR (1999) A tobacco syntaxin with a role in hormonal control of guard cell ion channels. Science **283:** 537–540

Liu SH, Marks MS, Brodsky FM (1998) A dominant-negative clathrin mutant differentially affects trafficking of molecules with distinct sorting motifs in the class II major histocompatibility complex (MHC) pathway. J Cell Biol **140:** 1023–1037

Liu SH, Wong ML, Craik CS, Brodsky FM (1995) Regulation of clathrin assembly and trimerization defined using recombinant triskelion hubs. Cell **83:** 257–267

Meckel T, Gall L, Semrau S, Homann U, Thiel G (2007) Guard cells elongate: relationship of volume and surface area during stomatal movement. Biophys J **92:** 1072–1080

Meckel T, Hurst AC, Thiel G, Homann U (2004) Endocytosis against high turgor: intact guard cells of Vicia faba constitutively endocytose fluorescently labelled plasma membrane and GFP-tagged K-channel KAT1. Plant J **39:** 182–193

Minguet-Parramona C, Wang Y, Hills A, Vialet-Chabrand S, Griffiths H, Rogers S, Lawson T, Lew VL, Blatt MR (2016) An optimal frequency in Ca^{2+} oscillations for stomatal closure is an emergent property of ion transport in guard cells. Plant Physiol **170:** 33–42

Murphy AS, Bandyopadhyay A, Holstein SE, Peer WA (2005) Endocytotic cycling of PM proteins. Annu Rev Plant Biol **56:** 221–251

Nebenführ A, Ritzenthaler C, Robinson DG (2002) Brefeldin A: deciphering an enigmatic inhibitor of secretion. Plant Physiol **130:** 1102–1108

North HM, Frey A, Boutin JP, Sotta B, Marion-Poll A (2005) Analysis of xanthophyll cycle gene expression during the adaptation of Arabidopsis to excess light and drought stress: changes in RNA steady-state levels do not contribute to short-term responses. Plant Sci **169:** 115–124

Plessis A, Cournol R, Effroy D, Silva Pérez V, Botran L, Kraepiel Y, Frey A, Sotta B, Cornic G, Leung J, et al (2011) New ABA-hypersensitive Arabidopsis mutants are affected in loci mediating responses to water deficit and Dickeya dadantii infection. PLoS ONE **6:** e20243

Puertollano R, Randazzo PA, Presley JF, Hartnell LM, Bonifacino JS (2001) The GGAs promote ARF-dependent recruitment of clathrin to the TGN. Cell **105:** 93–102

Richter S, Geldner N, Schrader J, Wolters H, Stierhof YD, Rios G, Koncz C, Robinson DG, Jürgens G (2007) Functional diversification of closely related ARF-GEFs in protein secretion and recycling. Nature **448:** 488–492

Robert S, Kleine-Vehn J, Barbez E, Sauer M, Paciorek T, Baster P, Vanneste S, Zhang J, Simon S, Čovanová M, et al (2010) ABP1 mediates auxin inhibition of clathrin-dependent endocytosis in Arabidopsis. Cell **143:** 111–121

Robinson DG, Langhans M, Saint-Jore-Dupas C, Hawes C (2008) BFA effects are tissue and not just plant specific. Trends Plant Sci **13:** 405–408

Rothman JE, Wieland FT (1996) Protein sorting by transport vesicles. Science **272:** 227–234

Sanderfoot A (2007) Increases in the number of SNARE genes parallels the rise of multicellularity among the green plants. Plant Physiol **144:** 6–17

Sanderfoot AA, Assaad FF, Raikhel NV (2000) The Arabidopsis genome: an abundance of soluble N-ethylmaleimide-sensitive factor adaptor protein receptors. Plant Physiol **124:** 1558–1569

Sechet J, Roux C, Plessis A, Effroy D, Frey A, Perreau F, Biniek C, Krieger-Liszkay A, Macherel D, North HM, et al (2015) The ABA-deficiency suppressor locus HAS2 encodes the PPR protein LOI1/MEF11 involved in mitochondrial RNA editing. Mol Plant **8:** 644–656

Shope JC, DeWald DB, Mott KA (2003) Changes in surface area of intact guard cells are correlated with membrane internalization. Plant Physiol **133:** 1314–1321

Sokolovski S, Hills A, Gay RA, Blatt MR (2008) Functional interaction of the SNARE protein NtSyp121 in Ca^{2+} channel gating, Ca^{2+} transients and ABA signalling of stomatal guard cells. Mol Plant **1:** 347–358

Sutter JU, Sieben C, Hartel A, Eisenach C, Thiel G, Blatt MR (2007) Abscisic acid triggers the endocytosis of the Arabidopsis KAT1 K^+ channel and its recycling to the plasma membrane. Curr Biol **17:** 1396–1402

Tahara H, Yokota E, Igarashi H, Orii H, Yao M, Sonobe S, Hashimoto T, Hussey PJ, Shimmen T (2007) Clathrin is involved in organization of mitotic spindle and phragmoplast as well as in endocytosis in tobacco cell cultures. Protoplasma **230:** 1–11

Tanaka H, Nodzyłski T, Kitakura S, Feraru MI, Sasabe M, Ishikawa T, Kleine-Vehn J, Kakimoto T, Friml J (2014) BEX1/ARF1A1C is required for BFA-sensitive recycling of PIN auxin transporters and auxin-mediated development in Arabidopsis. Plant Cell Physiol **55:** 737–749

Teh OK, Moore I (2007) An ARF-GEF acting at the Golgi and in selective endocytosis in polarized plant cells. Nature **448:** 493–496

Tyrrell M, Campanoni P, Sutter JU, Pratelli R, Paneque M, Sokolovski S, Blatt MR (2007) Selective targeting of plasma membrane and tonoplast traffic by inhibitory (dominant-negative) SNARE fragments. Plant J **51:** 1099–1115

Uemura T, Ueda T, Ohniwa RL, Nakano A, Takeyasu K, Sato MH (2004) Systematic analysis of SNARE molecules in Arabidopsis: dissection of the post-Golgi network in plant cells. Cell Struct Funct **29:** 49–65

Wang C, Yan X, Chen Q, Jiang N, Fu W, Ma B, Liu J, Li C, Bednarek SY, Pan J (2013) Clathrin light chains regulate clathrin-mediated trafficking, auxin signaling, and development in *Arabidopsis*. Plant Cell **25:** 499–516

Yang HM, Zhang XY, Wang GX, Zhang JH (2006) Water channels are involved in stomatal oscillations encoded by parameter-specific cytosolic calcium oscillations. J Integr Plant Biol **48:** 790–799

Yu Q, Zhang Y, Wang J, Yan X, Wang C, Xu J, Pan J (2016) Clathrin-mediated auxin efflux and maxima regulate hypocotyl hook formation and light-stimulated hook opening in Arabidopsis. Mol Plant **9:** 101–112